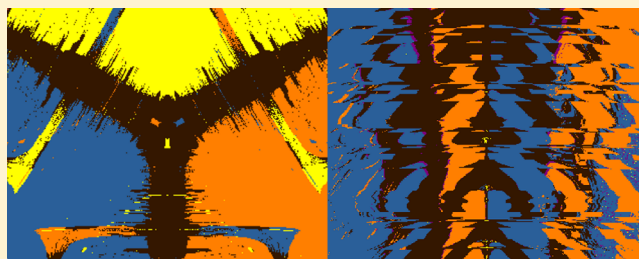


Visualizing Basins of Attraction for Different Minimization Algorithms

Daniel Asenjo, Jacob D. Stevenson,* David J. Wales, and Daan Frenkel

Department of Chemistry, University of Cambridge, Lensfield Road, Cambridge, CB2 1WE, United Kingdom

ABSTRACT: We report a study of the basins of attraction for potential energy minima defined by different minimization algorithms for an atomic system. We find that whereas some minimization algorithms produce compact basins, others produce basins with complex boundaries or basins consisting of disconnected parts. Such basins deviate from the “correct” basin of attraction defined by steepest-descent pathways, and the differences can be controlled to some extent by adjustment of the maximum step size. The choice of the most convenient minimization algorithm depends on the problem in hand. We show that while L-BFGS is the fastest minimizer, the FIRE algorithm is also quite fast and can lead to less fragmented basins of attraction.



■ INTRODUCTION

Optimization problems are ubiquitous in the physical sciences and beyond. In the simplest case optimization refers to the search for the minimum or maximum values of an objective function. Global optimization involves searching for the highest maximum or lowest minimum in a certain domain. In contrast, local optimization procedures identify the first minimum or maximum that is found by a given algorithm when starting from an arbitrary point in parameter space.

In the study of energy landscapes, the properties of stationary points and the connections between them are of central importance.¹ These stationary points represent key features of the landscape. In chemical reactions, saddle points are geometric transition states² along the reaction coordinate. Glassy systems are trapped in metastable states that correspond to relatively small numbers of connected local minima,^{3–5} and similarly, jammed states can also be viewed as local potential energy minima. In protein folding the native state corresponds to the global free energy minimum and the free energy landscape often involves funneling characteristics.⁶ The study of these minima and the pathways connecting them can be carried out using geometry optimization techniques,^{1,7} and local minimization is the focus of the current contribution.

When faced with the task of numerically optimizing a smooth function, there are many algorithms from which to choose. Which algorithm is best suited for the purpose depends on factors such as speed, memory usage, and ease of implementation. All approaches follow a general procedure starting with the user supplying an initial point, which can be an informed guess or an arbitrary point in parameter space. The algorithm generates a sequence of iterates that terminates when a solution is found within a predefined accuracy, such as when the gradient is near zero, or when the value of the function stops changing. Recent work has shown how convergence criteria can be chosen according to a certification procedure.⁸ Different algorithms have

different ways of proceeding from one iteration to the next. The formulations we consider involve the value of the function that is being optimized, its derivatives, and the results of previous iterations.

In general, two different algorithms can converge to different minima starting from the same initial conditions. We are interested in identifying the configuration space that leads to a particular minimum as a function of the optimization algorithm. This connection is important for applications such as calculation of thermodynamic properties using the superposition approach, where the global partition function is written as a sum over contributions of local minima.^{9–11} In this context, the steepest-descent algorithm occupies a unique position, since it defines basins of attraction¹² for local minima that cannot interpenetrate. This result follows because steepest-descent paths are defined using a linear first-order differential equation, for which the uniqueness theorem applies.¹³ However, steepest-descent minimization is very inefficient compared with more sophisticated algorithms, which are normally preferable. The latter methods generally employ nonlinear equations to determine the steps, and the corresponding basins of attraction can exhibit complex boundaries.^{14,15} In other words, when defined by steepest-descent, the basin of attraction has a deterministic boundary. In contrast, the basins for other algorithms can exhibit re-entrant, interpenetrating boundaries, as noted in previous work.^{14,15} For applications such as basin-hopping global optimization,^{16,17} this structure is probably unimportant. However, the simplicity of the boundaries associated with steepest-descent paths is relevant if we are interested in

Special Issue: Peter G. Wolynes Festschrift

Received: December 18, 2012

Revised: May 1, 2013

Published: May 9, 2013

partitioning the configuration space, for example when measuring the size of basins of attraction.¹⁸ In the present work, we regard the basins of attraction defined by steepest-descent as a reference to which other methods will be compared. The purpose of this paper is to make these comparisons rigorously and to provide criteria for choosing the most appropriate and convenient minimization algorithm for a given problem.

METHODS

The minimization algorithms considered here are steepest-descent, L-BFGS, FIRE, conjugate gradient, and BFGS (for a detailed description of different minimization techniques, see ref 19). The L-BFGS algorithm is tested using two different methods to determine the length of the steps. In the first approach, a line search routine is used to choose the step size. In the second approach, the step size guess of the L-BFGS algorithm is accepted subject to a maximum step size and the condition that the energy does not rise. This is the default procedure in the global optimization program GMIN²⁰ and the OPTIM program for locating transition states and analyzing pathways.²¹ We have only compared gradient-based minimizers in the present work, because they represent the most efficient class of algorithms.

Steepest-descent, sometimes referred to as gradient descent, uses the gradient as the search direction (this is the steepest direction). The step size can be chosen using a line search routine. In this paper, a fixed step size ($\Delta = 0.005$ in reduced units) is used for all of the steepest-descent calculations. It is worth noting that the definition of basins of attraction in the Introduction section applies to steepest-descent minimization in the limit of infinitesimal step size.

BFGS, named after its creators Broyden,²² Fletcher,²³ Goldfarb,²⁴ and Shanno,²⁵ is a quasi-Newtonian optimization method, which uses an approximate Hessian to determine the search direction. The approximate Hessian is built up iteratively from the history of steps and gradient evaluations. The implementation used in this paper is from SciPy²⁶ and uses a line search to determine a step size. The line search used is the Minpack2 method DCSRCH,²⁷ which attempts to find a step size that satisfies the Wolfe conditions. The maximum step size is fixed to be 50 times the initial guess returned by the BFGS algorithm.

L-BFGS is a limited memory version of the BFGS algorithm described above and was designed for large-scale problems, where storing the Hessian would be impractical. Rather than saving the full approximate Hessian in memory it only stores a history of M previous values of the function and its gradient with which it computes an approximation to the inverse diagonal components of the Hessian.²⁸ For a system with N variables, $O(N^2)$ memory and operations are needed when using BFGS, while L-BFGS scales as $O(MN)$, which is significantly smaller if $M \ll N$ and is linear in N . Two versions of L-BFGS were used in this paper. The first is from the SciPy²⁶ optimization library “L-BFGS-B”.^{29–31} This routine uses the same DCSRCH line search as the BFGS implementation, but with slightly different input parameters. For example, the maximum step size is adaptively updated. The second L-BFGS implementation is included in the GMIN²⁰ and OPTIM²¹ software packages and adapted from Liu and Nocedal.²⁸ In this version there is no line search. The step size returned by the L-BFGS algorithm is accepted subject to a maximum step size constraint and the condition that the energy

does not rise. In both of these versions, the diagonal components of the inverse Hessian are initially set to unity.

The fast inertial relaxation engine, known as FIRE, is a minimization algorithm based on ideas from molecular dynamics, with an extra velocity term and adaptive time step.³² Stated simply, the system state slides down the potential energy surface gathering “momentum” until the direction of the gradient changes, at which point it stops, resets, and resumes sliding.

The conjugate gradient method uses information about previous values of the gradient to determine a conjugate search direction.³³ It only stores the previous search direction. The implementation considered here is from SciPy,²⁶ and the step size is determined using same line search as the BFGS routine.

In order to test the accuracy of the minimizers, we use a three-particle system in which the interparticle interactions are given by a Lennard-Jones potential plus a three-body Axilrod–Teller term:^{34,35}

$$V = 4\epsilon \sum_{i < j} \left[\left(\frac{\sigma}{r_{ij}} \right)^{12} - \left(\frac{\sigma}{r_{ij}} \right)^6 \right] + Z \sum_{i < j < k} \left[\frac{1 + 3 \cos \theta_1 \cos \theta_2 \cos \theta_3}{(r_{ij} r_{ik} r_{jk})^3} \right] \quad (1)$$

Here θ_1 , θ_2 , and θ_3 are the internal angles of the triangle formed by particles i , j , and k , r_{ij} is the distance between particles i and j , and Z is the strength of the three-body term. We chose this three-particle system because for $Z > 0$ it has four local minima. It was important for us to choose a small system with only a few degrees of freedom in order to visualize the basins of attraction in two dimensions. In one of the minima, the atoms are arranged in an equilateral triangle, with point group D_{3h} . The other three linear minima have $D_{\infty h}$ symmetry and are related by permutations of the atoms. We use reduced units with one parameter, as in previous work:^{14,15,36,37}

$$Z^* = \frac{Z\sigma^9}{\epsilon} \quad (2)$$

Without loss of generality, we define the axes such that the three particles are in the xy plane with one particle at the origin, another along the x axis, and the third in the upper half plane. Now only the three internal coordinates r_{ij} are needed to describe the system. A projection onto the page was chosen to visualize the basins of attraction in such a way that the basins of the four minima are present in the plane.^{14,15} In internal coordinates, the projection plane is chosen to be perpendicular to the vector $\vec{n} = (1,1,1)$ at a distance $\sqrt{3}\alpha$ from the origin. Points in the plane have the property $r_{12} + r_{23} + r_{13} = 3\alpha$. We can define an arbitrary vector $\vec{v} = (0,0,1)$ so that the plane is spanned by the unit vectors

$$\hat{x}_2 = \frac{\vec{n} \times \vec{v}}{|\vec{n} \times \vec{v}|}, \quad \hat{x}_1 = \frac{\vec{n} \times \hat{x}_2}{|\vec{n} \times \hat{x}_2|} \quad (3)$$

The projection of an arbitrary vector $\vec{a} = (r_{12}, r_{23}, r_{13})$ onto the plane is $\vec{a}_p = (\vec{a} \cdot \hat{x}_1, \vec{a} \cdot \hat{x}_2)$. The equilateral triangle minimum is at the origin in terms of the projected coordinates x_1 and x_2 , as shown in Figure 1. For more details regarding the projection, see refs 14 and 15.

The following results were produced using the projection described above with $\alpha = \sqrt{3}R_e$, where $R_e = (2)^{1/6}\sigma$ is the Lennard-Jones equilibrium separation, and $Z^* = 2$. For this choice, there is a linear minimum with energy -2.219ϵ in

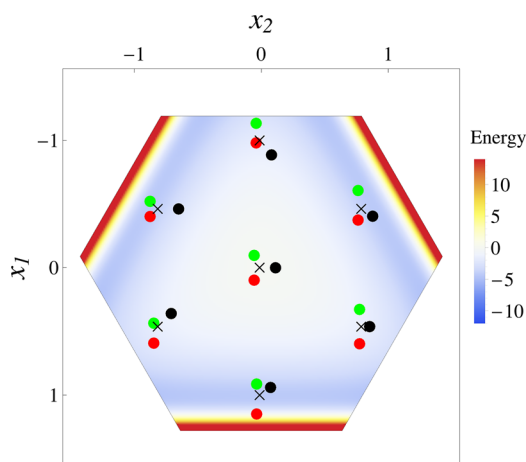


Figure 1. Projected plane in its own coordinate system. Points on this plane were used as the initial configurations for the minimizations. Examples of starting configurations are shown for several points marked by “x”. The plot is colored by the energy of the starting configuration.

addition to the equilateral triangle with energy -2.185ϵ . There are three distinct permutational isomers of the linear minimum, since any of the three atoms can reside in the central position. A 700×700 grid of initial points was taken with x_1 and x_2 between $-\alpha$ and α . All of the minimizations were terminated when the root-mean-square (RMS) gradient was smaller than 10^{-3} reduced units. Under some conditions, such geometry optimizations could appear to converge to a saddle point,³⁸ so the geometries were also checked, as well as the RMS gradient. As in previous work,^{14,15} each pixel in the resulting plots corresponds to a different initial configuration and is colored according to the minimum that is found after optimization.

The efficiency of each algorithm was also tested. Here we were not constrained to small systems by the need for visualization, so we chose a more interesting system size, namely 38 Lennard-Jones atoms. We measured the average number of function calls needed to get to the nearest local minimum from 1000 random starting configurations. The number of function calls is a fairer test than wall clock time because for most real world calculations computing the energy and gradient will be the time bottleneck and it avoids measuring differences in implementation efficiency. The results are reported in Table 2.

RESULTS AND DISCUSSION

Figure 2 shows the color scheme used to identify the results of local minimization in the subsequent figures. Forbidden geometry refers to the points in the plane that correspond to initial geometries that do not satisfy the triangle inequality or have excessively high energy. Failed quench means that the quenched coordinates are not close enough (according to a certain tolerance) to the equilateral triangle or linear configurations, that is, the algorithm failed to reach a minimum.³⁸

The figures that follow show the basins of attraction of the four minima described above determined using the different minimization techniques and parameters, as described in the Methods section. As expected, steepest-descent is the slowest (see Table 1), most robust minimizer, and it produces well-defined basin boundaries (Figure 2). This result holds as long as the step size is kept relatively small. Smaller step sizes are always more robust when using steepest-descent. The usual definition for the basin of attraction in the context of energy landscapes is the set of points in configuration space that converge to a certain

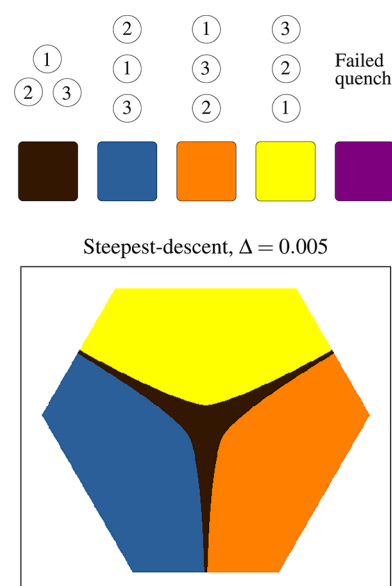


Figure 2. The lower panel shows the same (x_1, x_2) plane as Figure 1, which defines the starting configuration of the three particles that interact via the Lennard-Jones potential plus a three-body Axilrod–Teller term, as described in the Methods section. The plane is colored according to the final configuration after a steepest-descent minimization. The color coding is displayed in the upper panel. Black corresponds to the atoms in the D_{3h} triangle configuration, while blue, orange, and yellow correspond to the three possible linear configurations. A failed quench means that the final coordinates are not close enough (according to a certain tolerance) to the equilateral triangle or linear configurations. Δ is the maximum step size. This figure, corresponding to the steepest-descent results, will serve as our reference for comparing the other minimizers.

minimum for a steepest-descent quench.^{1,12} Hence this approach produces a useful reference against which to compare the other algorithms.

L-BFGS is the fastest algorithm tested here (see Table 2), although the basin boundaries are not always well-defined (see Figures 3 and 6). In the case of L-BFGS without line search, we can see that reducing the step size does not necessarily improve the definition of the basin boundaries. In this case, the resolution of the basin boundaries improves with increasing maximum step size until it reaches an optimum length, beyond which the resolution decreases. This effect is clearly visible in Table 1 and Figure 3. Removing the line search does not improve the resolution of the boundaries, but it does reduce the number of failed quenches. We tested the effect of changing the parameter M , the number of previous values of the function, and the gradient used to build the approximate Hessian. Increasing M between 1 and 10 makes the resolution of the basins worse (see Figure 3) but produces faster convergence (see Table 1). This result arises because increasing M increases the degree of nonlinearity of the algorithm.

Several values of the maximum step size for FIRE were tested. For a small value of the step size, the boundaries of the basins of attraction are well-defined and similar to the results for steepest-descent. The method only ends up in the wrong basin when starting from points that lie very close to the boundaries between two basins (Figure 4, top left). Using a larger value of the step size leads to many artifacts and failed quenches, which are evident in the bottom half of Figure 4.

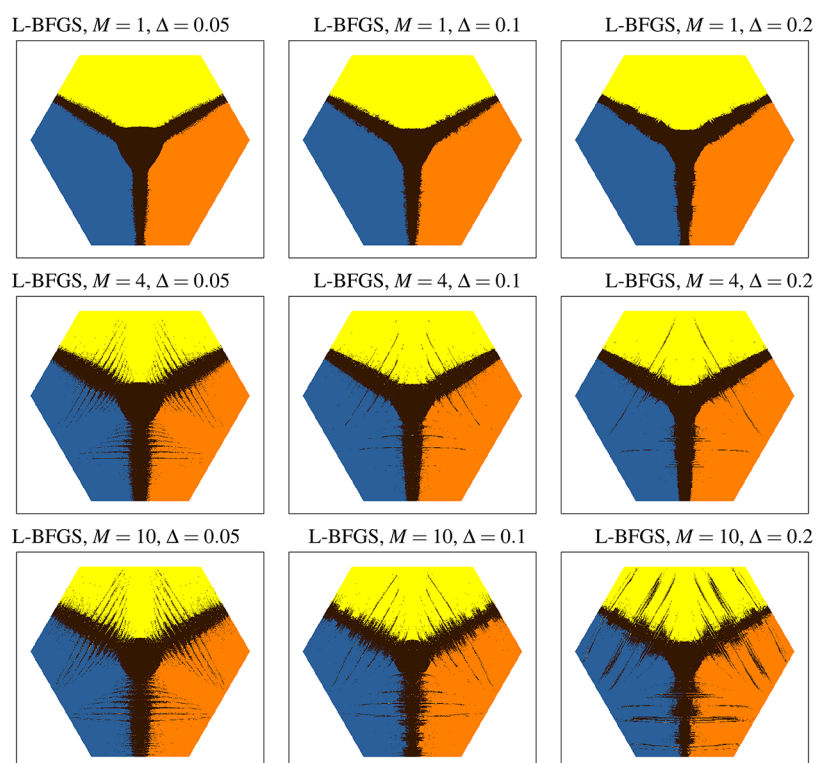


Figure 3. Results for the L-BFGS algorithm for different values of M (the number of previous steps used to construct the next step) and the maximum step size Δ . See Figure 2 for a detailed explanation of the figure.

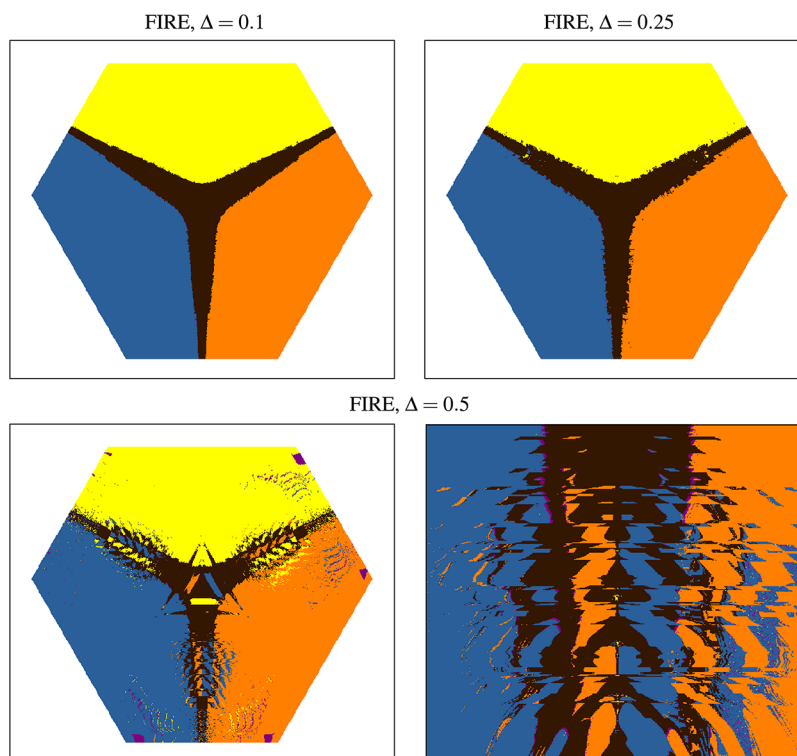


Figure 4. Results for the FIRE algorithm for several values of the maximum step size Δ . The bottom right panel is a magnification of a portion of the bottom left image. See Figure 2 for a detailed explanation of the figure.

Some other popular algorithms were also tested, namely, conjugate gradient (Figure 5) and BFGS (Figure 6). The SciPy implementation of these methods uses the same line search routine to determine the step size at each iteration, and both of

them produce similar ill-defined basin boundaries. In both cases, the boundary artifacts are caused by the line search returning a step size that is large enough to move into a different basin. Furthermore, the failed quenches at the edges are due to step

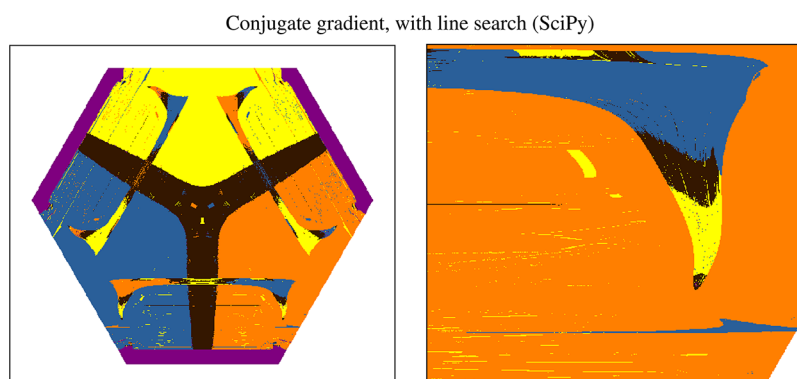


Figure 5. Results for the conjugate gradient algorithm with line search (SciPy implementation) are shown in the left panel. The right panel shows a magnification of the left panel. See Figure 2 for a detailed explanation of the figure.

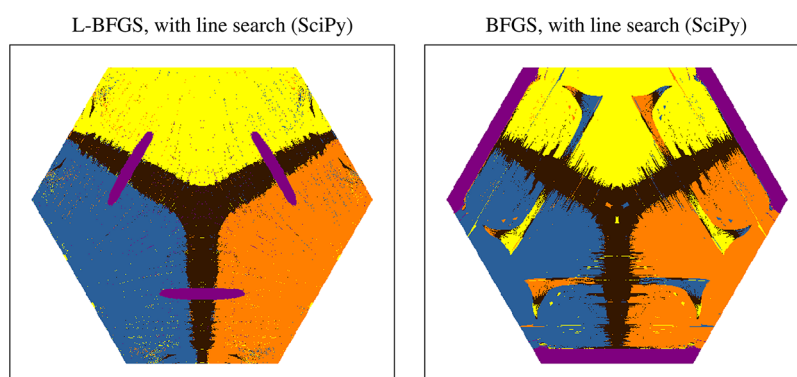


Figure 6. Results for L-BFGS and BFGS with line search (SciPy implementations). See Figure 2 for a detailed explanation of the figure.

sizes sufficiently large that particles end up so far apart that the gradient is small enough to satisfy the termination condition. The line search algorithm is not entirely responsible for the imprecise basin boundaries. The initial guess for the step size passed to the line search by the conjugate gradient and BFGS algorithms is often large enough to step to the next basin by itself. To check this effect, we have also tested this line search routine with the L-BFGS algorithm. The results (not shown for brevity) produce quite reasonable basin boundaries with most of the above artifacts absent. An interesting question is why the L-BFGS algorithm produces an accurate guess for the step size while BFGS tends to overestimate the step size. The answer, most likely, is that the initial Hessian in L-BFGS is scaled,²⁸ while in BFGS it is fixed to unity.

We wanted to test the effect of maximum step size on the conjugate gradient and BFGS algorithms; however the SciPy routines do not accept parameters for adjusting the maximum step size. We were able to introduce this adjustment by modifying the source code of the line search routine used in each case. With these modifications and a maximum step size of 0.1, the conjugate gradient routine produced reasonably accurate basin boundaries. The penalty for this improved precision was roughly 50% more function evaluations. We were not able to obtain significant improvements for the BFGS routine.

The basins of attraction determined by some of the methods mentioned above (in particular FIRE with a large step size, conjugate gradient, and BFGS) display complex structures, as shown in Figure 4 (bottom right) and Figure 5 (right). Here we can see that the basin boundaries still have structure, even as the length scale is reduced. As noted in previous work, the structure

may be fractal,^{14,15,39} although this possibility was not investigated in detail.

We have quantified the difference between the outcomes of the basin mapping for different minimizers by counting the number of starting structures for which we find a basin different

Table 1. Table Showing the Quantitative Analysis of the Basins of Attraction Defined by Different Minimizers for the Three-Body System

| algorithm | parameters ^a | err ^b (%) |
|-------------------------|-------------------------|----------------------|
| L-BFGS (without LS) | $M = 1, \Delta = 0.05$ | 6.41 |
| | $M = 1, \Delta = 0.1$ | 6.46 |
| | $M = 1, \Delta = 0.2$ | 7.16 |
| | $M = 4, \Delta = 0.05$ | 14.75 |
| | $M = 4, \Delta = 0.1$ | 10.84 |
| | $M = 4, \Delta = 0.2$ | 10.13 |
| | $M = 10, \Delta = 0.05$ | 16.78 |
| | $M = 10, \Delta = 0.1$ | 12.72 |
| L-BFGS (SciPy, with LS) | $M = 10, \Delta = 0.2$ | 14.81 |
| | $M = 10$ | 12.79 |
| | $\Delta = 0.1$ | 3.68 |
| FIRE | $\Delta = 0.25$ | 4.53 |
| | $\Delta = 0.5$ | 11.23 |
| | | 23.45 |
| BFGS (SciPy, with LS) | | 22.93 |
| CG (SciPy, with LS) | | 0.00 |
| steepest-descent | $\Delta = 0.001$ | |

^a Δ is the maximum step size, and M is the length of the history used by L-BFGS, as defined in the Methods section. ^bErr is the percentage of starting configurations that minimized to a different minimum compared to the steepest-descent method.

from the one obtained using steepest-descent, as shown in Table 1. This difference corresponds to the number of different structures (from a total of 170 607 valid starting structures) when comparing the minimum produced by the corresponding algorithm with the minimum produced by steepest-descent (Figure 2).

Table 2 reports the performance of the algorithms tested here in terms of the average number of times that the energy and the

Table 2. Benchmarks for the Algorithms Tested in This Paper in Terms of the Average Number of Function Calls (FCs) Needed to Minimize a 38-Particle Lennard-Jones System from a Random Configuration^a

| algorithm | parameters | ⟨FCs⟩ |
|-------------------------|------------------------|-------|
| L-BFGS (without LS) | $M = 1, \Delta = 0.1$ | 273 |
| | $M = 4, \Delta = 0.05$ | 369 |
| | $M = 4, \Delta = 0.1$ | 241 |
| | $M = 4, \Delta = 0.2$ | 225 |
| | $M = 10, \Delta = 0.1$ | 228 |
| | $M = 20, \Delta = 0.1$ | 216 |
| L-BFGS (SciPy, with LS) | $M = 10$ | 215 |
| FIRE | $\Delta = 0.1$ | 822 |
| | $\Delta = 0.5$ | 3185 |
| BFGS (SciPy, with LS) | | 1233 |
| CG (SciPy, with LS) | | 837 |
| steepest-descent | $\Delta = 0.001$ | 31672 |

^aThe stopping condition is that the maximum force on any atom is less than 0.01 in reduced units.

force were evaluated (FCs). The average is taken over a sample of 1000 random initial states for a 38-particle Lennard-Jones cluster. The number of evaluations ultimately determines the time it takes to find a minimum, because this is generally the most time-consuming part of any minimization algorithm. We can see that L-BFGS is the fastest and FIRE is about 3–4 times slower, while steepest-descent is orders of magnitude slower, as expected.

CONCLUSIONS

In this paper, we have mapped the basins of attraction of a simple system onto a plane to compare a number of minimization algorithms. We are able to compare the different approaches both visually and quantitatively, building upon previous work, where the focus was mainly on transition state searches.^{14,15} Some of the more complex algorithms (CG, BFGS, L-BFGS, and FIRE) depending on the choice of parameters produce basins that consist of disconnected parts. Such basins deviate from the “correct” basin of attraction defined by steepest-descent pathways, especially at the basin boundaries, where complex interpenetrating patterns can appear. These patterns generally do not disappear as the length scale is reduced, as can be seen in Figures 4 and 5, making the basins ill-defined. In particular, we have found that overestimates for the step size are primarily responsible for the complex basin boundaries. Imposing a maximum step size can mitigate this problem for some algorithms, at the cost of slightly higher computational effort and an additional, system dependent, parameter. An appropriate value for the maximum step size can be chosen based on length scales in the system: for atomic systems, a good choice is about one tenth of the interatomic pair equilibrium distance.

In conclusion, if assignment of a starting configuration to the basin of attraction defined by steepest-descent is important, then FIRE may be the most convenient algorithm, due to its speed and

precision, provided that an acceptable maximum step size is chosen. If finding a minimum quickly is more important, then L-BFGS is clearly the best choice.

AUTHOR INFORMATION

Corresponding Author

*E-mail: js850@cam.ac.uk.

Notes

The authors declare no competing financial interest.

ACKNOWLEDGMENTS

The authors thank Dr Victor Rühle for many useful discussions and acknowledge funding from EPSRC Programme Grants EP/I001352/1 and EP/I00844/1, ERC Advanced Grants RG59508 and 227758, Marie Curie Grant 275544, Wolfson Merit Award 502011.K701/JE, and Becas Chile CONICYT.

REFERENCES

- (1) Wales, D. J. *Energy Landscapes: With Applications to Clusters, Biomolecules and Glasses*; Cambridge University Press: Cambridge, U.K., 2003.
- (2) Murrell, J. N.; Laidler, K. J. Symmetries of Activated Complexes. *Trans. Faraday Soc.* **1968**, *64*, 371–377.
- (3) Kirkpatrick, T. R.; Thirumalai, D.; Wolynes, P. G. Scaling Concepts for the Dynamics of Viscous Liquids near an Ideal Glassy State. *Phys. Rev. A* **1989**, *40*, 1045.
- (4) Doliwa, B.; Heuer, A. Energy Barriers and Activated Dynamics in a Supercooled Lennard-Jones Liquid. *Phys. Rev. E* **2003**, *67*, No. 031506.
- (5) de Souza, V. K.; Wales, D. J. Energy Landscapes for Diffusion: Analysis of Cage-breaking Processes. *J. Chem. Phys.* **2008**, *129*, No. 164507.
- (6) Wolynes, P.; Onuchic, J.; Thirumalai, D. Navigating the folding routes. *Science* **1995**, *267*, 1619–1620.
- (7) Wales, D. J.; Bogdan, T. V. Potential Energy and Free Energy Landscapes. *J. Phys. Chem. B* **2006**, *110*, 20765–20776.
- (8) Mehta, D.; Hauenstein, J. D.; Wales, D. J. Certifying the Potential Energy Landscape. *J. Chem. Phys.* **2013**, *138*, No. 171101.
- (9) Wales, D. J. Coexistence in Small Inert-gas Clusters. *Mol. Phys.* **1993**, *78*, 151–171.
- (10) Doye, J. P. K.; Wales, D. J. An Order-Parameter Approach to Coexistence in Atomic Clusters. *J. Chem. Phys.* **1995**, *102*, 9673–9688.
- (11) Strodel, B.; Wales, D. J. Free Energy Surfaces from an Extended Harmonic Superposition Approach and Kinetics for Alanine Dipeptide. *Chem. Phys. Lett.* **2008**, *466*, 105–115.
- (12) Mezey, P. G. Catchment Region Partitioning of Energy Hypersurfaces. I. *Theor. Chim. Acta* **1981**, *58*, 309.
- (13) Pechukas, P. On Simple Saddle Points of a Potential Surface, the Conservation of Nuclear Symmetry along Paths of Steepest Descent, and the Symmetry of Transition States. *J. Chem. Phys.* **1976**, *64*, 1516.
- (14) Wales, D. J. Basins of Attraction for Stationary Points on a Potential-Energy Surface. *J. Chem. Soc., Faraday Trans.* **1992**, *88*, 653.
- (15) Wales, D. J. Locating Stationary Points for Clusters in Cartesian Coordinates. *J. Chem. Soc., Faraday Trans.* **1993**, *89*, 1305.
- (16) Wales, D. J.; Doye, J. P. K. Global Optimization by Basin-Hopping and the Lowest Energy Structures of Lennard-Jones Clusters Containing up to 110 Atoms. *J. Phys. Chem. A* **1997**, *101*, 5111–5116.
- (17) Li, Z.; Scheraga, H. A. Monte Carlo-Minimization Approach to the Multiple-Minima Problem in Protein Folding. *Proc. Natl. Acad. Sci. U.S.A.* **1987**, *84*, 6611.
- (18) Xu, N.; Frenkel, D.; Liu, A. J. Direct Determination of the Size of Basins of Attraction of Jammed Solids. *Phys. Rev. Lett.* **2011**, *106*, No. 245502.
- (19) Nocedal, J.; Wright, S. *Numerical Optimization*; Springer Science +Business Media: New York, NY, U.S.A., 1999.
- (20) Wales, D. J. GMIN: A Program for Finding Global Minima and Calculating Thermodynamic Properties from Basin-sampling. <http://www-wales.ch.cam.ac.uk/GMIN/>.

- (21) Wales, D. J. OPTIM: A Program for Optimising Geometries and Calculating Pathways. <http://www-wales.ch.cam.ac.uk/OPTIM/>
- (22) Broyden, C. G. The Convergence of a Class of Double-rank Minimization Algorithms 1. General Considerations. *IMA J. Appl. Math.* **1970**, *6*, 76–90.
- (23) Fletcher, R. A New Approach to Variable Metric Algorithms. *Comput. J.* **1970**, *13*, 317–322.
- (24) Goldfarb, D. A Family of Variable-Metric Methods Derived by Variational Means. *Math. Comput.* **1970**, *24*, 23–26.
- (25) Shanno, D. F. Conditioning of Quasi-Newton Methods for Function Minimization. *Math. Comput.* **1970**, *24*, 647–656.
- (26) Jones, E.; Oliphant, T.; Peterson, P. SciPy: Open source Scientific Tools for Python, <http://www.scipy.org/>, 2001.
- (27) More, J. J.; Thuente, D. J. Line Search Algorithms with Guaranteed Sufficient Decrease. *ACM Trans. Math. Software* **1994**, *20*, 286–307.
- (28) Liu, D. C.; Nocedal, J. On the Limited Memory BFGS method for Large Scale Optimization. *Math. Program.* **1989**, *45*, 503–528.
- (29) Zhu, C.; Byrd, R. H.; Lu, P.; Nocedal, J. Algorithm 778. L-BFGS-B: Fortran Subroutines for Large-Scale Bound Constrained Optimization. *ACM Trans. Math. Software* **1997**, *23*, 550–560.
- (30) Byrd, R.; Lu, P.; Nocedal, J.; Zhu, C. A Limited Memory Algorithm for Bound Constrained Optimization. *SIAM J. Sci. Comput.* **1995**, *16*, 1190–1208.
- (31) Morales, J. L.; Nocedal, J. Remark on “Algorithm 778: L-BFGS-B: Fortran Subroutines for Large-Scale Bound Constrained Optimization”. *ACM Trans. Math. Software* **2011**, *38*, 7:1–7:4.
- (32) Bitzek, E.; Koskinen, P.; Gähler, F.; Moseler, M.; Gumbusch, P. Structural Relaxation Made Simple. *Phys. Rev. Lett.* **2006**, *97*, No. 170201.
- (33) Hestenes, M. R.; Stiefel, E. Methods of Conjugate Gradients for Solving Linear Systems. *J. Res. Natl. Bur. Stand. (U. S.)* **1952**, *49*, 409–436.
- (34) Lennard-Jones, J. E. On the Determination of Molecular Fields. II. From the Equation of State of a Gas. *Proc. R. Soc. A* **1924**, *106*, 463–477.
- (35) Axilrod, B. M.; Teller, E. Interaction of the van der Waals Type between Three Atoms. *J. Chem. Phys.* **1943**, *11*, 299–300.
- (36) Wales, D. J. Structural and Topological Consequences of Anisotropic Interactions in Clusters. *J. Chem. Soc., Faraday Trans.* **1990**, *86*, 3505–3517.
- (37) Doye, J. P. K.; Wales, D. J. Systematic Investigation of the Structures and Rearrangements of 6-Atom Clusters Bound by a Model Anisotropic Potential. *J. Chem. Soc., Faraday Trans.* **1992**, *88*, 3295–3304.
- (38) Uppenbrink, J.; Wales, D. J. When Do Gradient Optimizations Converge to Saddle-Points? *Chem. Phys. Lett.* **1992**, *190*, 447–452.
- (39) Grebogi, C.; Ott, E.; Yorke, J. A. Chaos, Strange Attractors, and Fractal Basin Boundaries in Nonlinear Dynamics. *Science* **1987**, *238*, 632–638.